SUPPORTING INFORMATION

Removal of alkylation DNA adducts from N^2-alkylguanine and N^4-alkylcytosine by the adaptive response protein AlkB

Deyu Li, Bogdan I. Fedeles, Nidhi Shrivastav, James C. Delaney, Xuedong Yang, Cintyu Wong, Catherine L. Drennan, and John M. Essigmann*

Corresponding Author
*E-mail: jessig@mit.edu

Table of Contents

Figure S9. ESI-TOF mass spectrum from incubation of FF with the AlkB protein. Data represent mass/charge (*m/z*) values for the -4 charge envelope of the 16mer containing FF-2H.

Figure S10. ESI-TOF mass spectrum from incubation of HF without the AlkB protein. Data represent mass/charge (*m/z*) values for the -4 charge envelope of the 16mer containing HF.

Figure S11. ESI-TOF mass spectrum from incubation of HF with the AlkB protein. Data represent mass/charge (*m/z*) values for the -4 charge envelope of the 16mer containing G.

Figure S12. ESI-TOF mass spectrum from incubation of HF with the AlkB protein. Data represent mass/charge (*m/z*) values for the -4 charge envelope of the 16mer containing FF-2H and FF.

Figure S13. ESI-TOF mass spectrum from incubation of HF with the AlkB protein. Data represent mass/charge (*m/z*) values for the -4 charge envelope of the 16mer containing HO-FF.

Figure S14. ESI-TOF mass spectrum from incubation of m4C without the AlkB protein. Data represent mass/charge (*m/z*) values for the -4 charge envelope of the 16mer containing m4C.

Figure S15. ESI-TOF mass spectrum from incubation of m4C without the AlkB protein. Data represent mass/charge (*m/z*) values for the -4 charge envelope of the 16mer containing U (not C).

Figure S16. ESI-TOF mass spectrum from incubation of m4C with the AlkB protein. Data represent mass/charge (*m/z*) values for the -4 charge envelope of the 16mer containing C.

Figure S17. ESI-TOF mass spectrum from incubation of m4C with the AlkB protein. Data represent mass/charge (*m/z*) values for the -4 charge envelope of the 16mer containing m4C.

Figure S18. MS/MS fragmentation spectrum of 16mer containing m2G (unreacted starting material) in the reaction of m2G with AlkB.

Figure S19. MS/MS fragmentation spectrum of 16mer containing G (repair product) in the reaction of m2G with AlkB.

Figure S20. MS/MS fragmentation spectrum of 16mer containing e2G (unreacted starting material) in the reaction of e2G with AlkB.

Figure S21. MS/MS fragmentation spectrum of 16mer containing G (repair product) in the reaction of e2G with AlkB.

Figure S22. MS/MS fragmentation spectrum of 16mer containing FF (unreacted starting material) in the reaction of FF with AlkB.

Table S9. Predicted and observed *m/z* for MS/MS fragmentation patterns displayed in Figure S25 of G 16mer in the reaction of HF with AlkB.

Table S10. Predicted and observed *m/z* for MS/MS fragmentation patterns displayed in Figure S26 of HO-HF 16mer in the reaction of HF with AlkB.

Table S11. Predicted and observed *m/z* for MS/MS fragmentation patterns displayed in Figure S27 of m4C 16mer in the reaction of m4C with AlkB.

Table S12. Predicted and observed *m/z* for MS/MS fragmentation patterns displayed in Figure S28 of C 16mer in the reaction of m4C with AlkB.

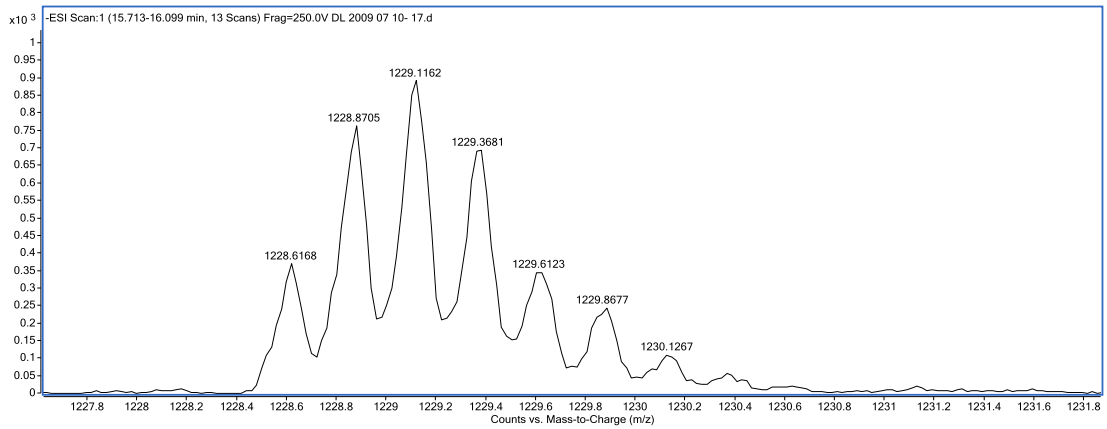

Figure S1. ESI-TOF mass spectrum from incubation of m2G without the AlkB protein. Data represent mass/charge (*m/z*) values for the -4 charge envelope of the 16mer containing m2G (Scheme 1a and Figure 1a).

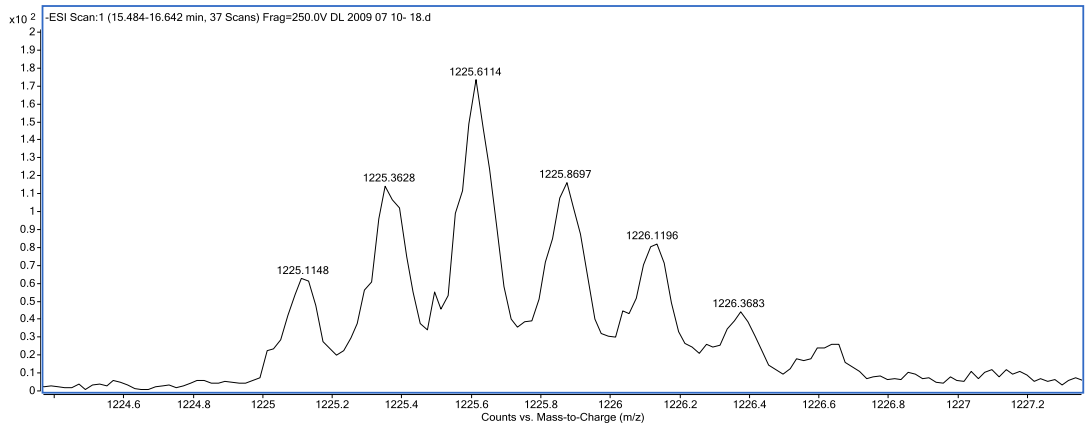

Figure S2. ESI-TOF mass spectrum from incubation of m2G with the AlkB protein. Data represent mass/charge (*m/z*) values for the -4 charge envelope of the 16mer containing G (Scheme 1a and Figure 1b).

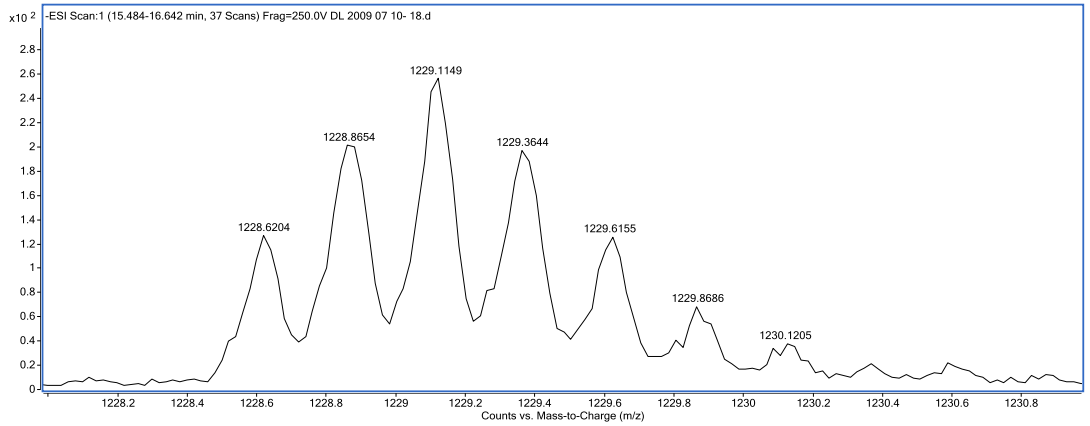

Figure S3. ESI-TOF mass spectrum from incubation of m2G with the AlkB protein. Data represent mass/charge (*m/z*) values for the -4 charge envelope of the 16mer containing m2G (Scheme 1a and Figure 1b).

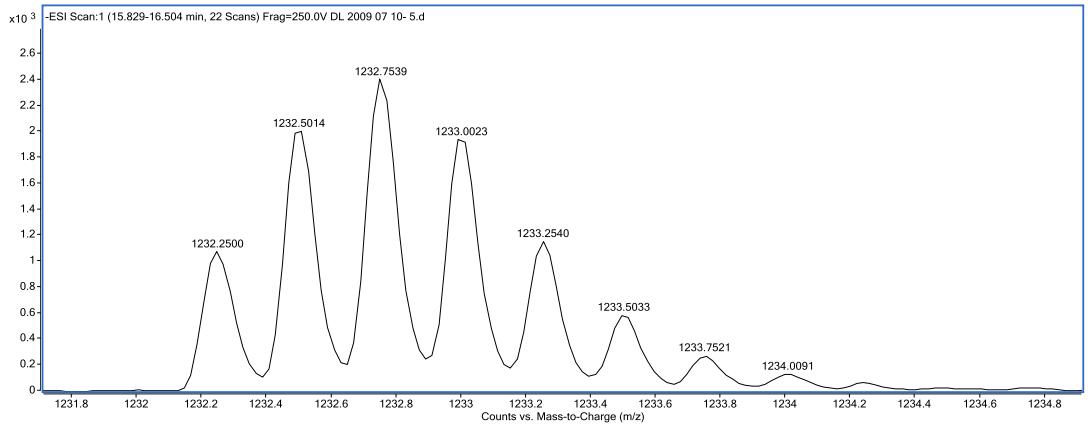

Figure S4. ESI-TOF mass spectrum from incubation of e2G without the AlkB protein. Data represent mass/charge (*m/z*) values for the -4 charge envelope of the 16mer containing e2G (Scheme 1b and Figure 1c).

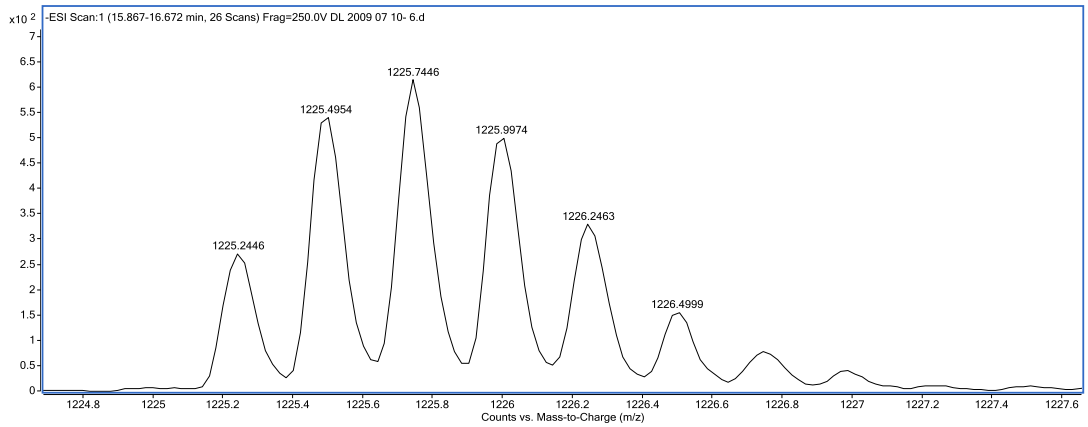

Figure S5. ESI-TOF mass spectrum from incubation of e2G with the AlkB protein. Data represent mass/charge (*m/z*) values for the -4 charge envelope of the 16mer containing G (Scheme 1b and Figure 1d).

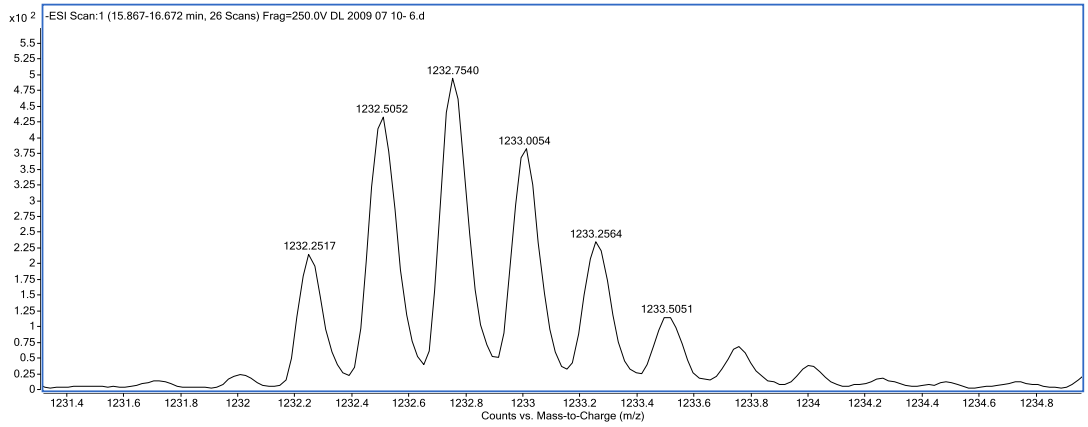

Figure S6. ESI-TOF mass spectrum from incubation of e2G with the AlkB protein. Data represent mass/charge (*m/z*) values for the -4 charge envelope of the 16mer containing e2G (Scheme 1b and Figure 1d).

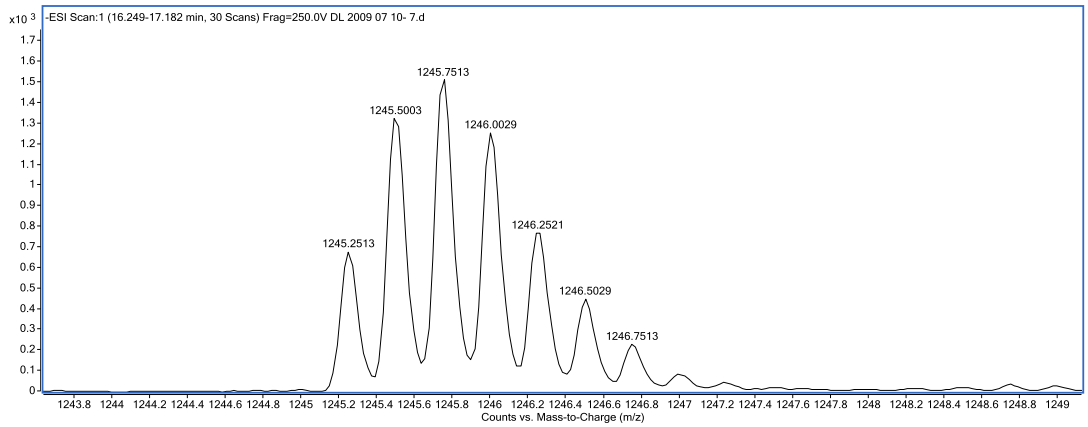

Figure S7. ESI-TOF mass spectrum from incubation of FF without the AlkB protein. Data represent mass/charge (*m/z*) values for the -4 charge envelope of the 16mer containing FF (Scheme 1c and Figure 1e).

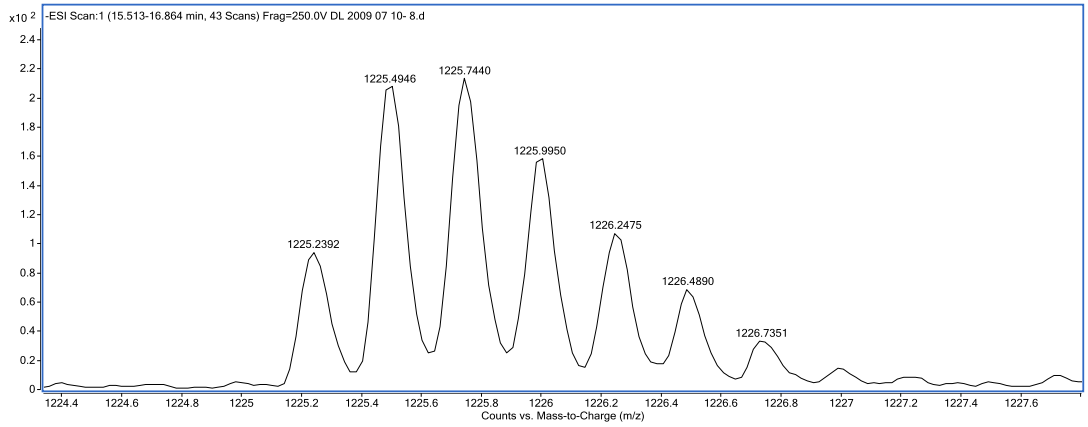

Figure S8. ESI-TOF mass spectrum from incubation of FF with the AlkB protein. Data represent mass/charge (*m/z*) values for the -4 charge envelope of the 16mer containing G (Scheme 1c and Figure 1f).

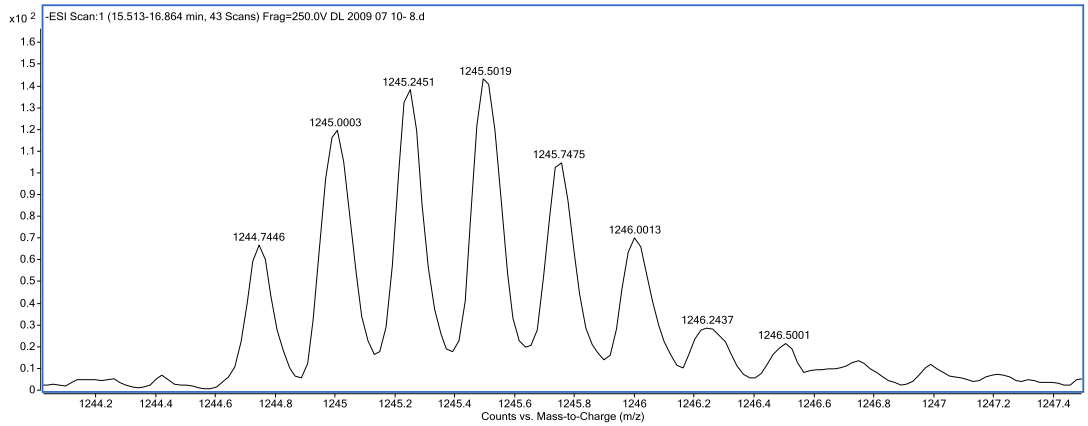

Figure S9. ESI-TOF mass spectrum from incubation of FF with the AlkB protein. Data represent mass/charge (*m/z*) values for the -4 charge envelope of the 16mer containing FF-2H (Scheme 1c and Figure 1f).

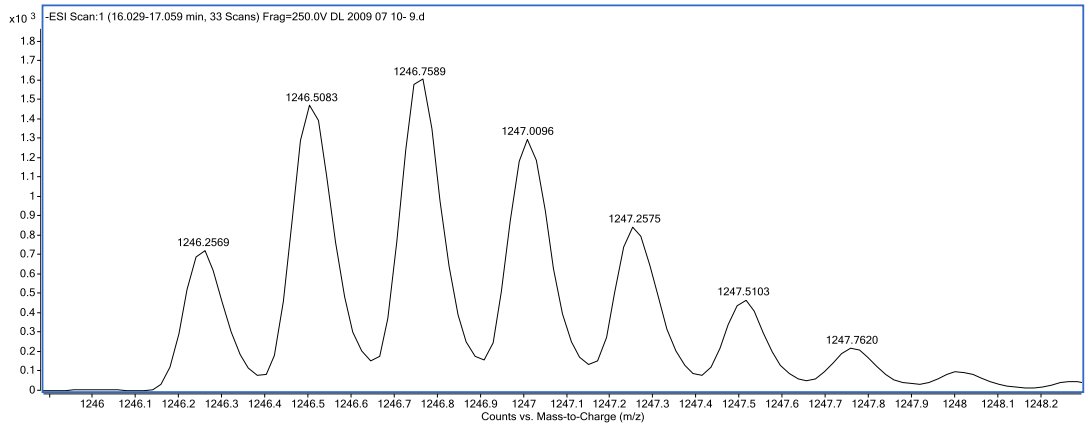

Figure S10. ESI-TOF mass spectrum from incubation of HF without the AlkB protein. Data represent mass/charge (*m/z*) values for the -4 charge envelope of the 16mer containing HF (Scheme 1d and Figure 1g).

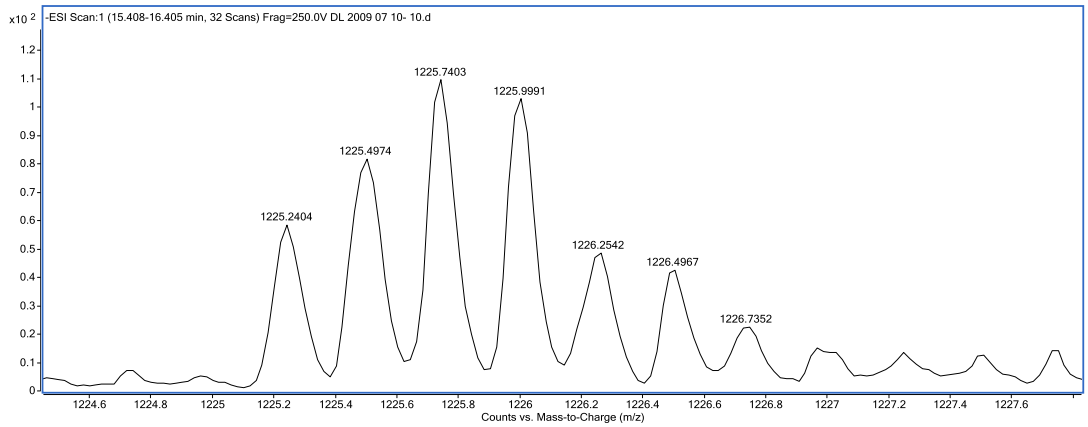

Figure S11. ESI-TOF mass spectrum from incubation of HF with the AlkB protein. Data represent mass/charge (*m/z*) values for the -4 charge envelope of the 16mer containing G (Scheme 1d and Figure 1h).

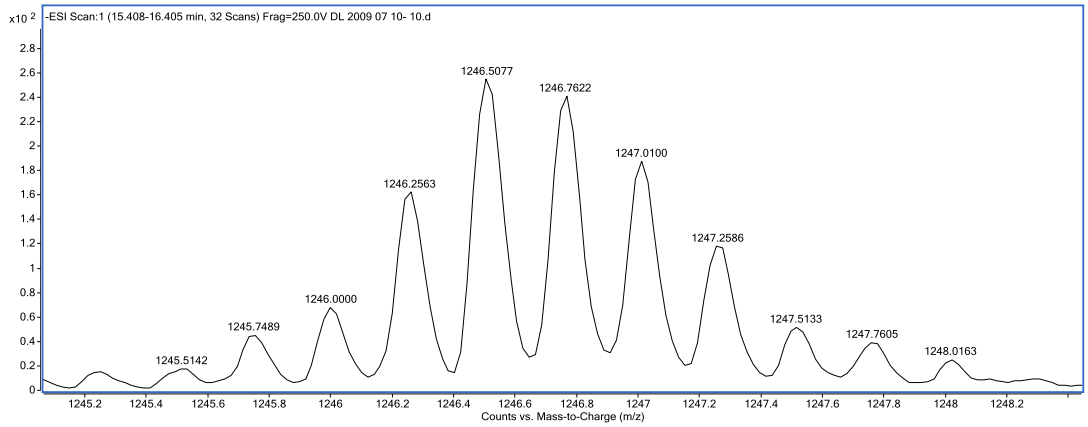

Figure S12. ESI-TOF mass spectrum from incubation of HF with the AlkB protein. Data represent mass/charge (*m/z*) values for the -4 charge envelope of the 16mer containing FF-2H and FF (Scheme 1d and Figure 1h).

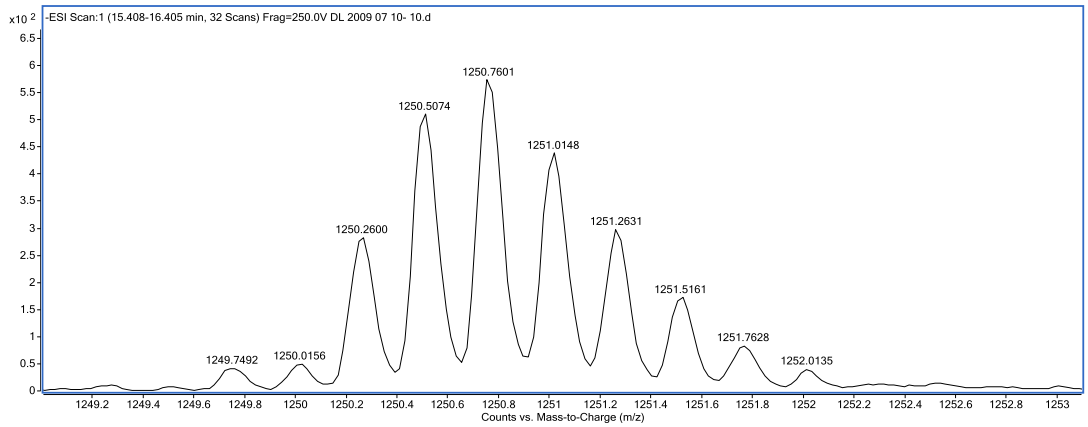

Figure S13. ESI-TOF mass spectrum from incubation of HF with the AlkB protein. Data represent mass/charge (*m/z*) values for the -4 charge envelope of the 16mer containing HO-FF (Scheme 1d and Figure 1h).

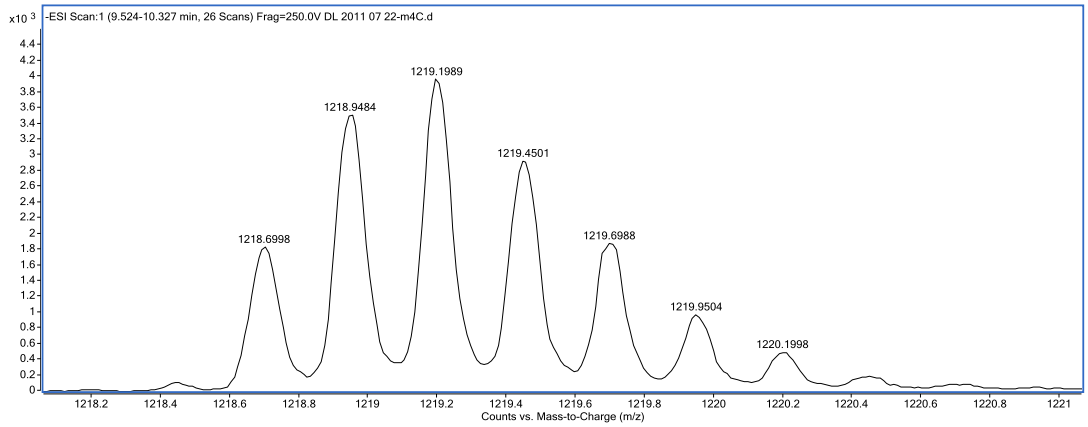

Figure S14. ESI-TOF mass spectrum from incubation of m4C without the AlkB protein. Data represent mass/charge (*m/z*) values for the -4 charge envelope of the 16mer containing m4C (Scheme 1e and Figure 1i).

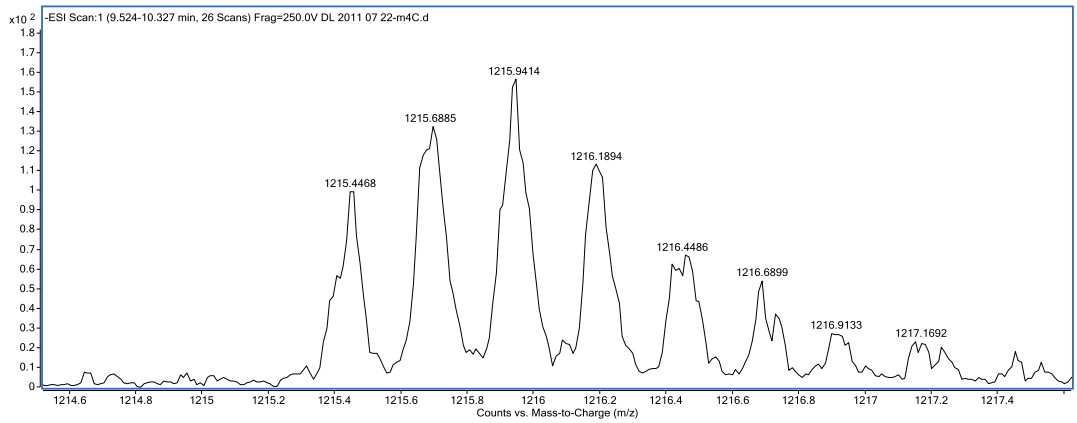

Figure S15. ESI-TOF mass spectrum from incubation of m4C without the AlkB protein. Data represent mass/charge (*m/z*) values for the -4 charge envelope of the 16mer containing U (not C) (Scheme 1e and Figure 1i).

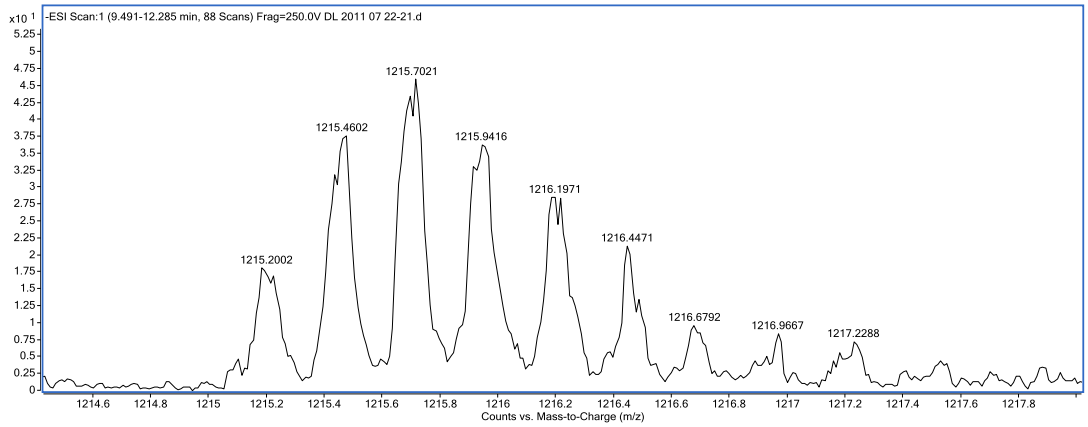

Figure S16. ESI-TOF mass spectrum from incubation of m4C with the AlkB protein. Data represent mass/charge (*m/z*) values for the -4 charge envelope of the 16mer containing C (Scheme 1e and Figure 1j).

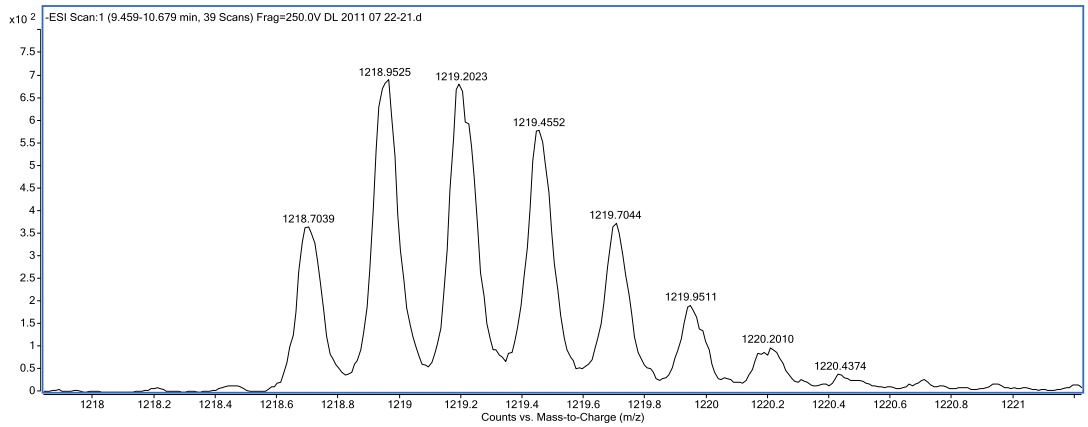

Figure S17. ESI-TOF mass spectrum from incubation of m4C with the AlkB protein. Data represent mass/charge (*m/z*) values for the -4 charge envelope of the 16mer containing m4C (Scheme 1e and Figure 1j).

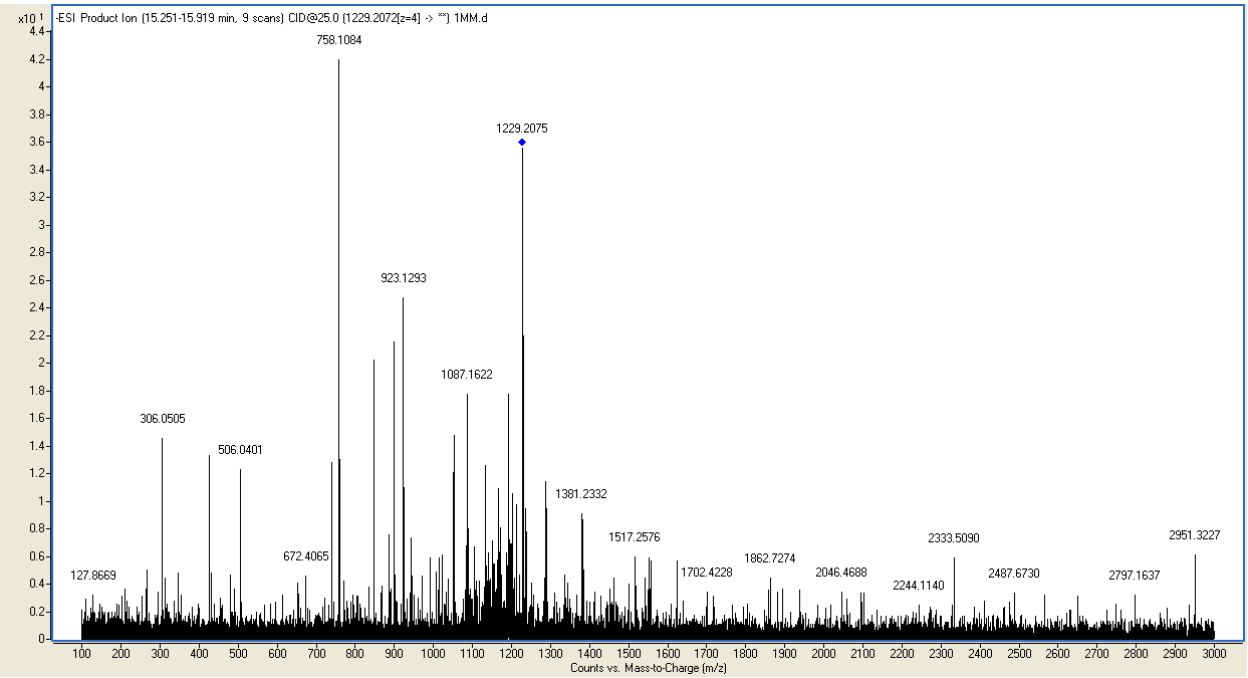

Figure S18. MS/MS fragmentation spectrum of 16mer containing m2G (unreacted starting material) in the reaction of m2G with AlkB. The blue diamond marks the parent ion.

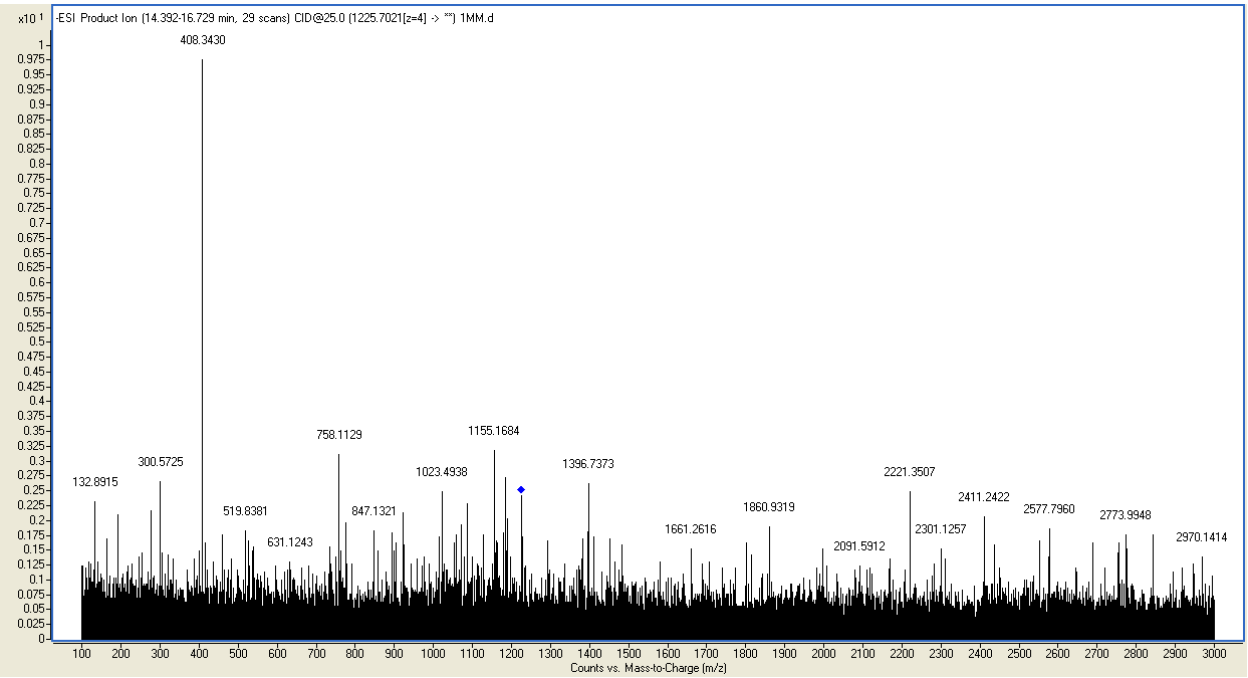

Figure S19. MS/MS fragmentation spectrum of 16mer containing G (repair product) in the reaction of m2G with AlkB. The blue diamond marks the parent ion.

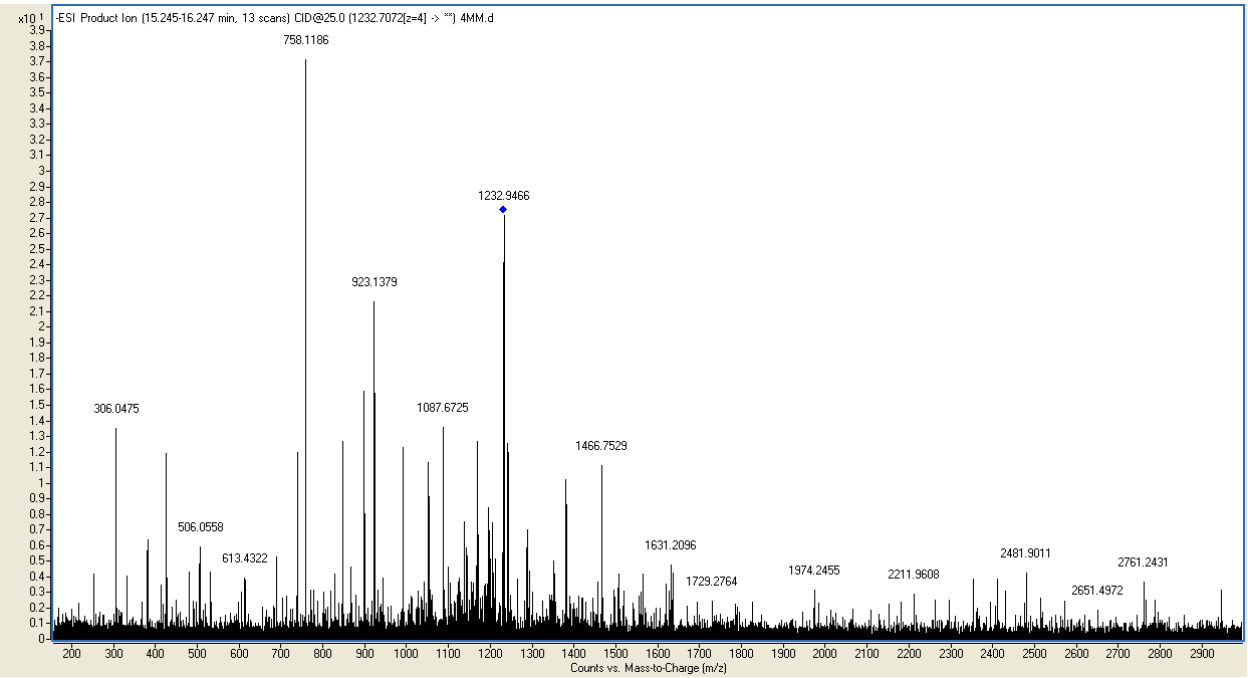

Figure S20. MS/MS fragmentation spectrum of 16mer containing e2G (unreacted starting material) in the reaction of e2G with AlkB. The blue diamond marks the parent ion.

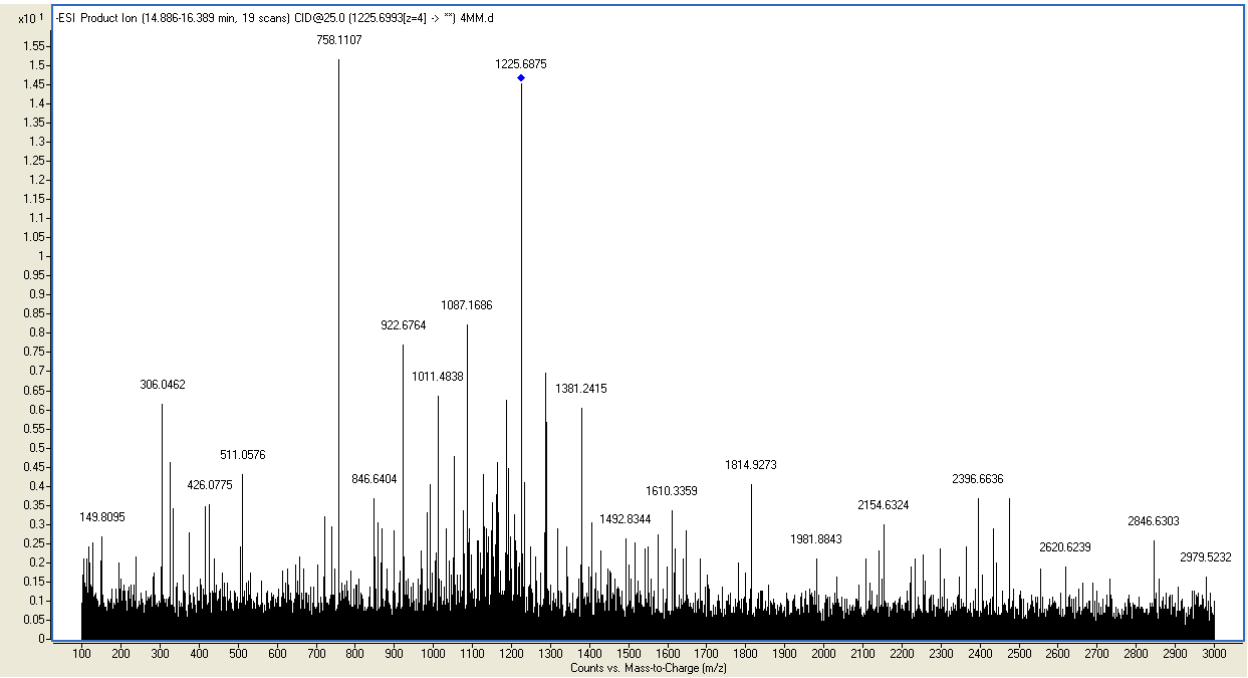

Figure S21. MS/MS fragmentation spectrum of 16mer containing G (repair product) in the reaction of e2G with AlkB. The blue diamond marks the parent ion.

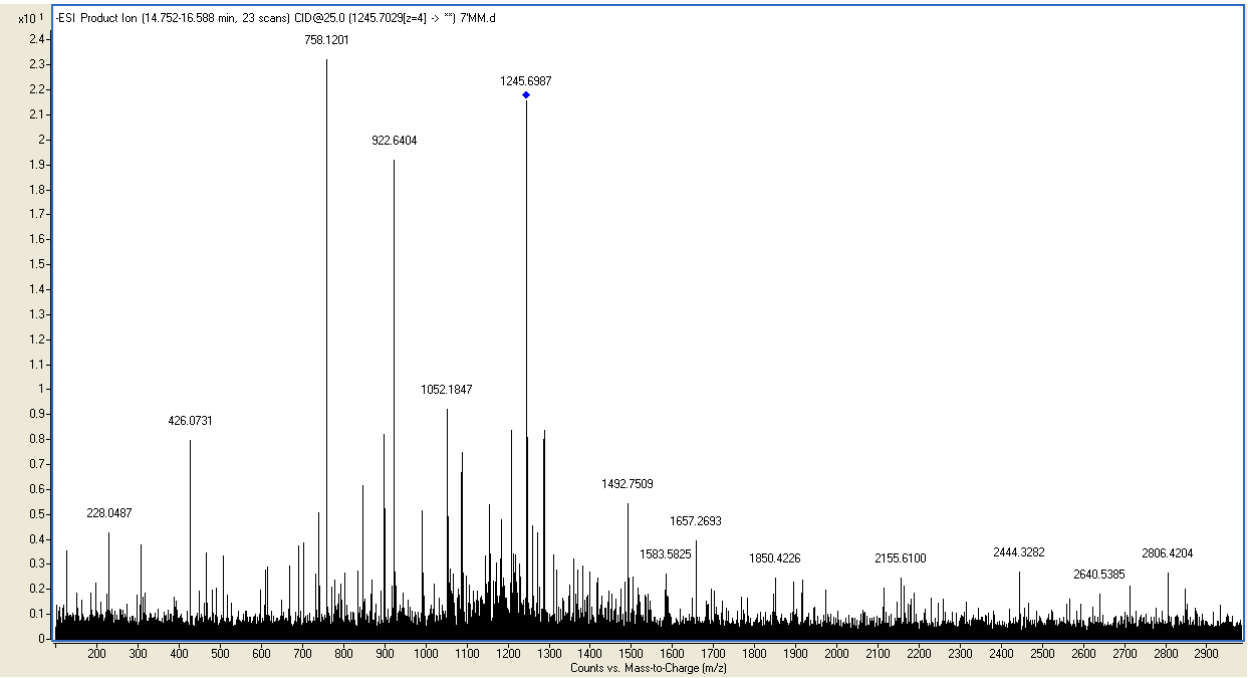

Figure S22. MS/MS fragmentation spectrum of 16mer containing FF (unreacted starting material) in the reaction of FF with AlkB. The blue diamond marks the parent ion.

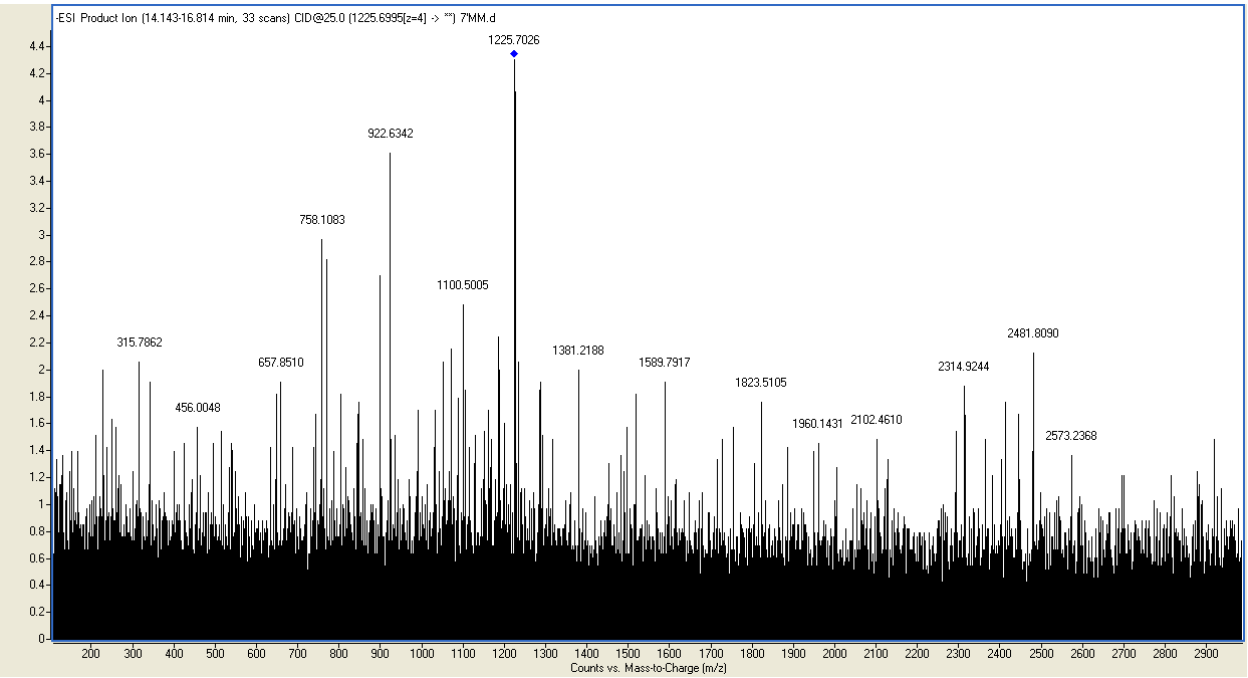

Figure S23. MS/MS fragmentation spectrum of 16mer containing G (repair product) in the reaction of FF with AlkB. The blue diamond marks the parent ion.

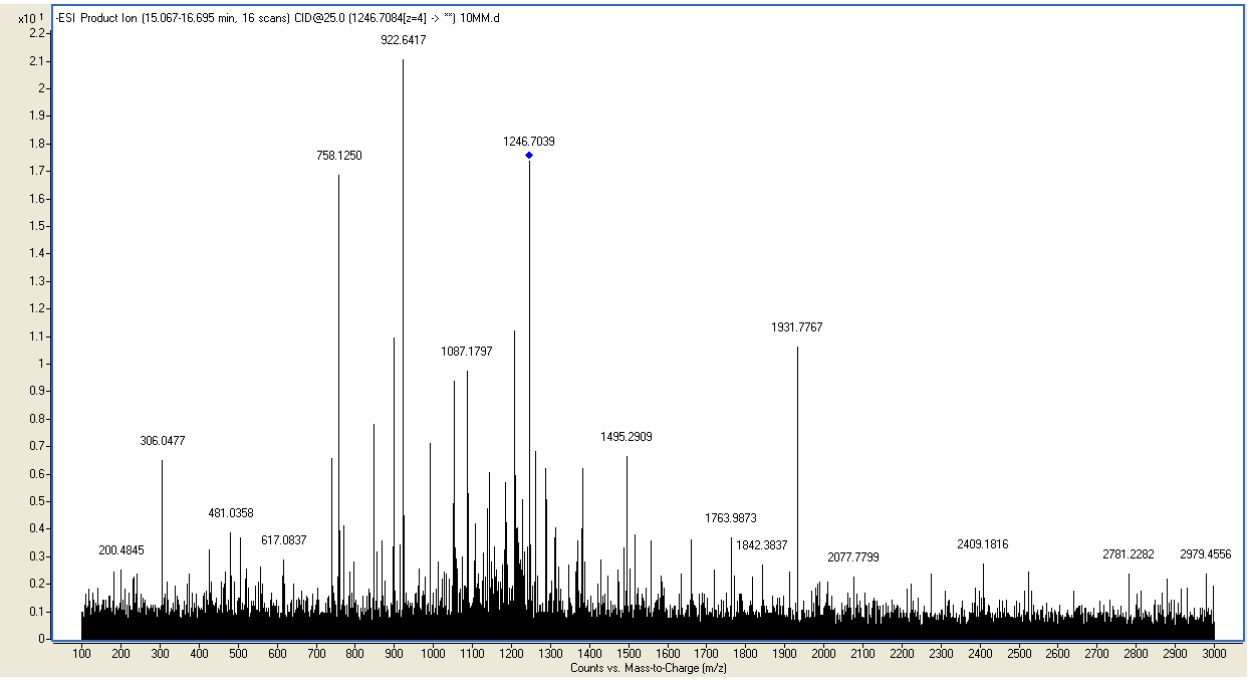

Figure S24. MS/MS fragmentation spectrum of 16mer containing HF (unreacted starting material) in the reaction of HF with AlkB. The blue diamond marks the parent ion.

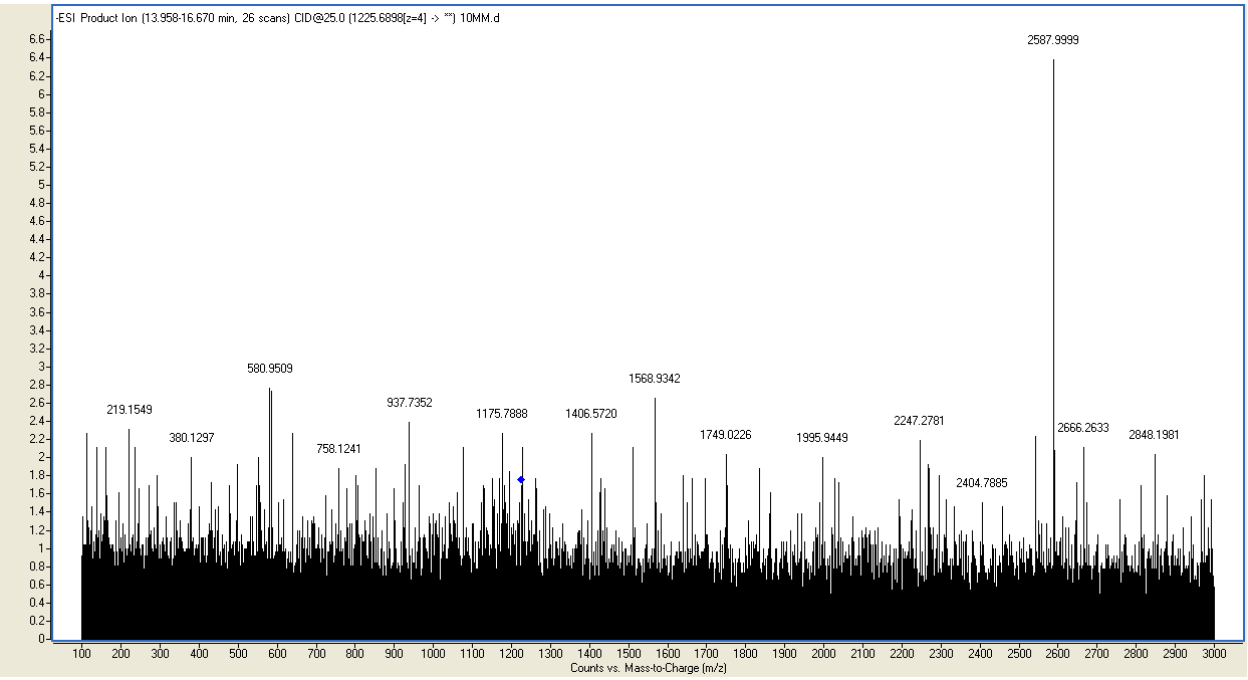

Figure S25. MS/MS fragmentation spectrum of 16mer containing G (repair product) in the reaction of HF with AlkB. The blue diamond marks the parent ion.

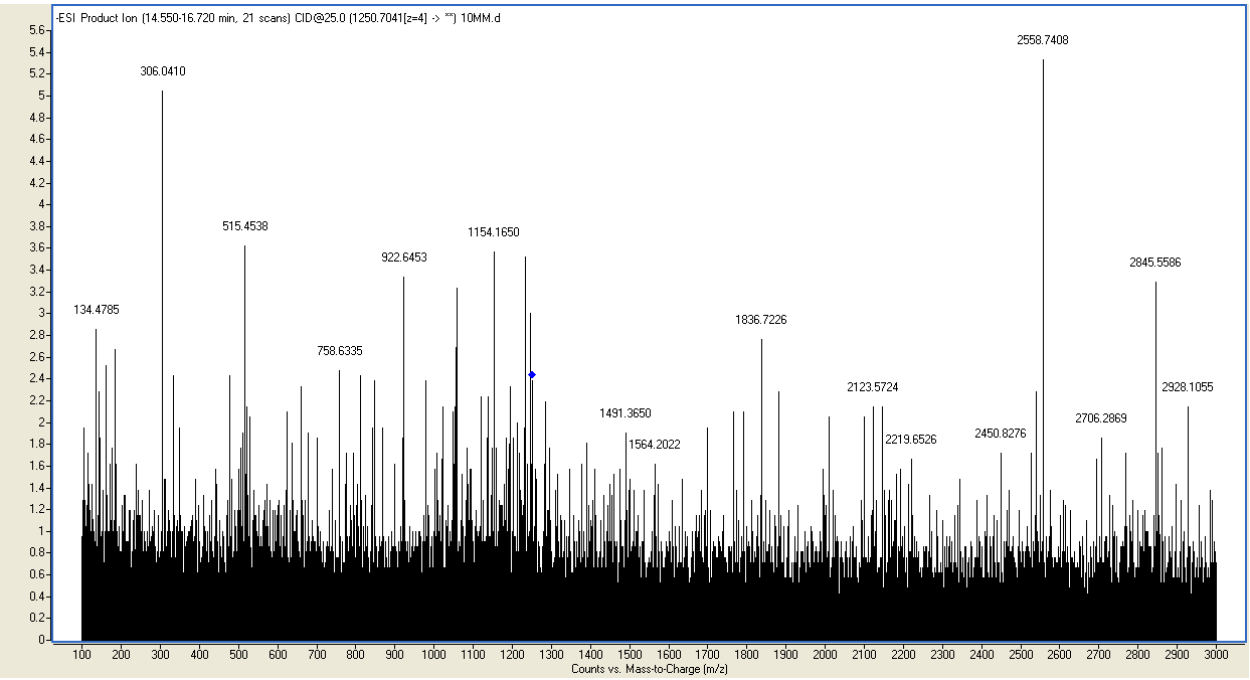

Figure S26. MS/MS fragmentation spectrum of 16mer containing HO-HF (repair intermediate) in the reaction of HF with AlkB. The blue diamond marks the parent ion.

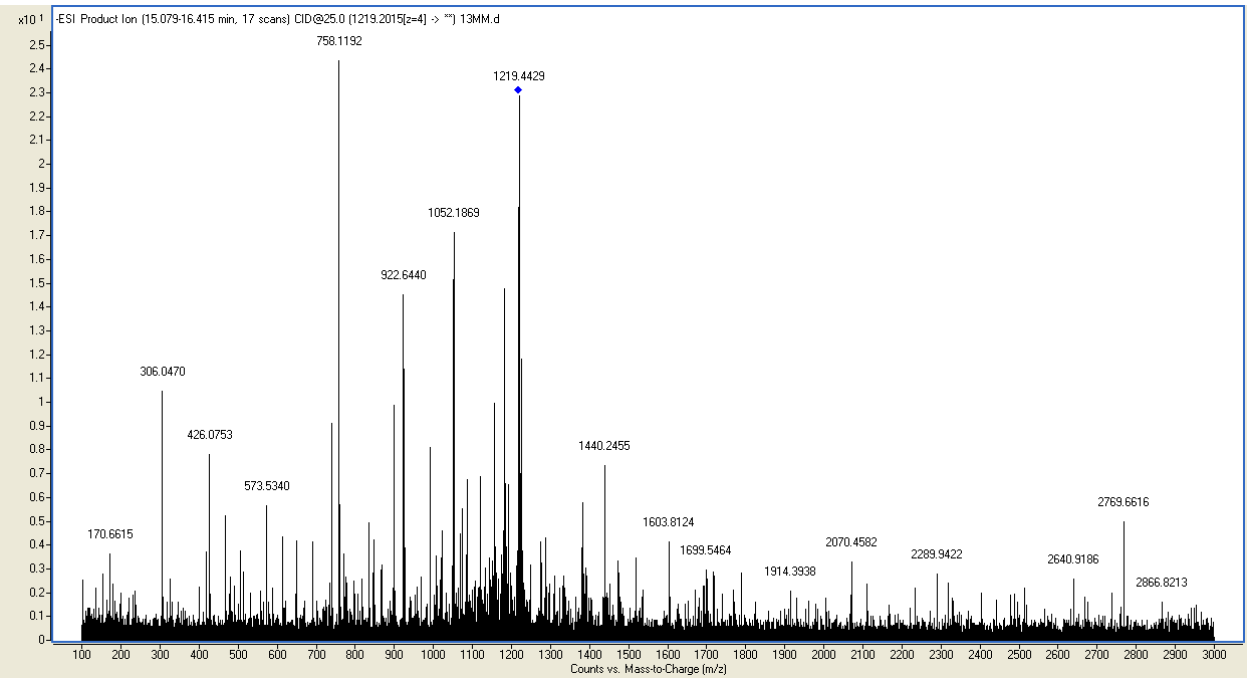

Figure S27. MS/MS fragmentation spectrum of 16mer containing m4C (unreacted starting material) in the reaction of m4C with AlkB. The blue diamond marks the parent ion.

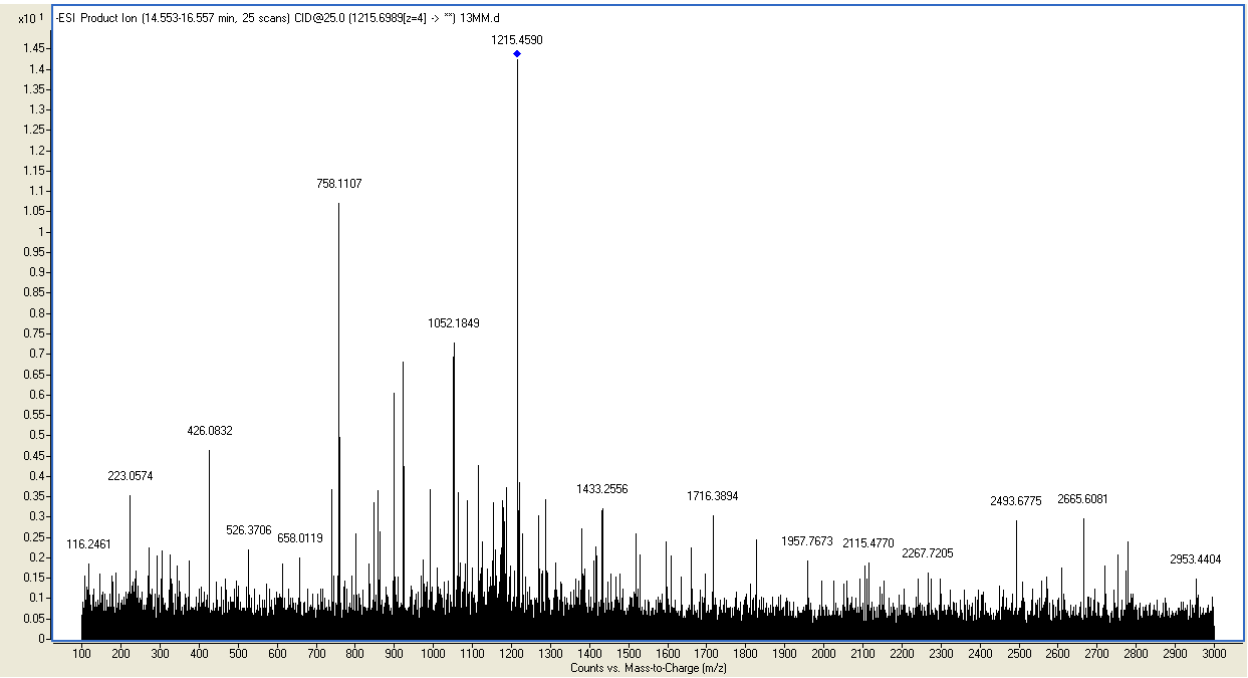

Figure S28. MS/MS fragmentation spectrum of 16mer containing C (repair product) in the reaction of m4C with AlkB. The blue diamond marks the parent ion.

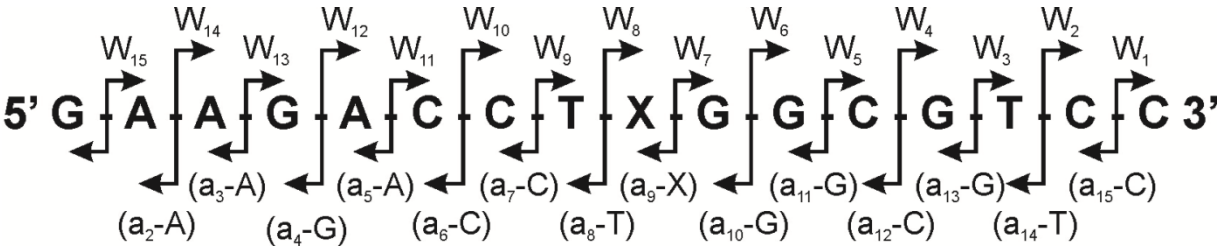

Figure S29. Predicted collision-induced dissociation (CID) fragmentation pattern of the 16mer oligonucleotide. X denotes the lesion or repair reaction intermediate or product. The *m/z* theoretical values of the CID fragments, calculated using Mongo Oligo Mass Calculator v2.06 (http://library.med.utah.edu/masspec/mongo.htm) are shown in Table S2-S12.

Table S1. Percentage of lesion repair by AlkB in 1h in ssDNA and dsDNA.

Lesion	Complementary Base	Repair in ssDNA (%)	Repair in dsDNA (%)
m2G	C	7.8	1.2
e2G	C	31.9	1.0
FF	C	8.7	0.0
HF	C	2.6	0.4
m4C	G	37.7	0.0
m1A	T	21.0	23.7

Table S2. Predicted and observed *m/z* for MS/MS fragmentation patterns displayed in Figure S18 of m2G 16mer in the reaction of m2G with AlkB. Predicted CID fragments are shown in Figure S29.

Fragment	**Charge**	**Theoretical *m/z***	**Observed *m/z***
W1	-1	306.048	306.051
W2	-1	595.094	595.076
W3	-1	899.139	899.129
W4	-2	613.592	613.568
W5	-2	758.115	758.108
W6	-2	922.641	922.627
W7	-2	1087.167	1087.162
W8	-2	1258.701	1258.709
W9	-2	1410.723	1410.787
W10	-3	1036.495	1036.471
W11	-3	1132.844	1132.862
W12	-3	1237.196	1237.200
W14	-4	1088.172	1088.138
W15	-4	1166.437	1166.432
a2-A	-1	426.080	426.075
a3-A	-1	739.137	739.153
a4-G	-1	1052.195	1052.187
a5-A	-1	1381.247	1381.233
a6-C	-2	846.648	846.635
a7-C	-2	991.171	991.162
a8-T	-2	1135.694	1135.666
a9-X	-2	1287.717	1287.732
a10-G	-2	1459.251	1459.183
a11-G	-2	1623.777	1623.742
a13-G	-3	1288.214	1288.202

Table S3. Predicted and observed *m/z* for MS/MS fragmentation patterns displayed in Figure S19 of G 16mer in the reaction of m2G with AlkB. Predicted CID fragments are shown in Figure S29.

Fragment	**Charge**	**Theoretical *m/z***	**Observed *m/z***
W3	-1	899.139	899.133
W5	-2	758.115	758.113
W6	-2	922.641	922.629
W7	-2	1087.167	1087.192
W10	-3	1031.823	1031.860
W11	-3	1128.172	1128.191
W12	-4	924.141	924.117
W13	-4	1006.404	1006.304
W14	-4	1084.668	1084.625
a2-A	-1	426.080	426.077
a3-A	-1	739.137	739.151
a5-A	-2	690.119	690.119
a6-C	-2	846.648	846.617
a7-C	-2	991.171	991.128
a8-T	-3	756.793	756.558
a9-X	-3	858.142	858.138
a10-G	-3	967.826	967.826
a12-C	-3	1187.194	1187.151
a13-G	-3	1283.543	1283.523
a14-T	-3	1393.227	1393.330
a15-C	-3	1494.575	1494.545

Table S4. Predicted and observed *m/z* for MS/MS fragmentation patterns displayed in Figure S20 of e2G 16mer in the reaction of e2G with AlkB. Predicted CID fragments are shown in Figure S29.

Fragment	**Charge**	**Theoretical *m/z***	**Observed *m/z***
W1	-1	306.048	306.048
W3	-1	899.139	899.138
W4	-2	613.592	613.432
W5	-2	758.115	758.119
W6	-2	922.641	922.641
W7	-2	1087.167	1087.192
W8	-2	1265.709	1265.452
W9	-2	1417.731	1417.741
W10	-3	1041.167	1041.196
W11	-3	1137.516	1137.522
W12	-3	1241.868	1241.845
W13	-3	1351.552	1351.574
W14	-4	1091.676	1091.489
W15	-4	1169.941	1169.943
a2-A	-1	426.080	426.080
a3-A	-1	739.137	739.148
a4-G	-1	1052.195	1052.206
a5-A	-1	1381.247	1381.254
a6-C	-2	846.648	846.652
a7-C	-2	991.171	991.167
a9-X	-2	1287.717	1287.711
a10-G	-2	1466.259	1466.266
a11-G	-2	1630.785	1630.793
a12-C	-3	1196.538	1196.552
a13-G	-3	1292.886	1292.731
a14-T	-3	1402.570	1402.406

Table S5. Predicted and observed *m/z* for MS/MS fragmentation patterns displayed in Figure S21 of G 16mer in the reaction of e2G with AlkB. Predicted CID fragments are shown in Figure S29.

Fragment	**Charge**	**Theoretical *m/z***	**Observed *m/z***
W1	-1	306.048	306.046
W3	-1	899.139	899.157
W4	-2	613.592	613.602
W5	-2	758.115	758.111
W6	-2	922.641	922.676
W7	-2	1087.167	1087.169
W8	-2	1251.693	1251.833
W9	-2	1403.716	1403.734
W10	-3	1031.823	1031.844
W11	-3	1128.172	1128.180
W12	-4	924.141	924.145
W13	-4	1006.404	1006.383
W14	-3	1446.561	1446.456
W15	-4	1162.933	1162.879
a2-A	-1	426.080	426.078
a3-A	-1	739.137	739.145
a4-G	-1	1052.195	1052.217
a5-A	-1	1381.247	1381.242
a6-C	-2	846.648	846.640
a7-C	-2	991.171	991.169
a8-T	-2	1135.694	1135.683
a9-X	-3	858.142	858.096
a11-G	-3	1077.510	1077.563
a13-G	-3	1283.543	1283.536
a15-C	-4	1120.679	1120.686

Table S6. Predicted and observed *m/z* for MS/MS fragmentation patterns displayed in Figure S22 of FF 16mer in the reaction of FF with AlkB. Predicted CID fragments are shown in Figure S29.

Fragment	**Charge**	**Theoretical *m/z***	**Observed *m/z***
W1	-1	306.048	306.042
W3	-1	899.139	899.149
W4	-1	1228.192	1228.224
W5	-2	758.115	758.120
W6	-2	922.641	922.640
W7	-2	1087.167	1087.174
W9	-2	1443.729	1443.695
W10	-3	1058.499	1058.502
W11	-3	1154.847	1154.837
W12	-3	1259.200	1259.184
W13	-3	1368.884	1368.665
W14	-4	1104.675	1104.539
W15	-4	1182.939	1182.921
a2-A	-1	426.080	426.073
a3-A	-1	739.137	739.147
a4-G	-1	1052.195	1052.185
a6-C	-2	846.648	846.650
a7-C	-2	991.171	991.185
a8-T	-3	756.793	756.602
a9-X	-2	1287.717	1287.730
a10-G	-3	994.501	994.457
a11-G	-3	1104.185	1104.215
a12-C	-3	1213.869	1213.705
a13-G	-3	1310.218	1310.551

Table S7. Predicted and observed *m/z* for MS/MS fragmentation patterns displayed in Figure S23 of G 16mer in the reaction of FF with AlkB. Predicted CID fragments are shown in Figure S29.

Fragment	**Charge**	**Theoretical *m/z***	**Observed *m/z***
W1	-1	306.048	306.036
W3	-1	899.139	899.140
W4	-2	613.592	613.576
W5	-2	758.115	758.108
W6	-2	922.641	922.634
W7	-2	1087.167	1087.179
W8	-2	1251.693	1251.725
W9	-2	1403.716	1403.651
W10	-3	1031.823	1031.743
W11	-3	1128.172	1128.167
W13	-4	1006.404	1006.654
W14	-3	1446.561	1446.583
W15	-4	1162.933	1163.003
a2-A	-1	426.080	426.091
a3-A	-1	739.137	739.133
a4-G	-1	1052.195	1052.184
a5-A	-1	1381.247	1381.219
a6-C	-2	846.648	846.633
a7-C	-2	991.171	991.122
a8-T	-2	1135.694	1135.873
a9-X	-2	1287.717	1287.724
a10-G	-2	1452.243	1452.240
a11-G	-3	1077.510	1077.490
a12-C	-3	1187.194	1187.189
a13-G	-3	1283.543	1283.613

Table S8. Predicted and observed *m/z* for MS/MS fragmentation patterns displayed in Figure S24 of HF 16mer in the reaction of HF with AlkB. Predicted CID fragments are shown in Figure S29.

Fragment	**Charge**	**Theoretical *m/z***	**Observed *m/z***
W1	-1	306.048	306.048
W3	-1	899.139	899.144
W4	-2	613.592	613.603
W5	-2	758.115	758.125
W6	-2	922.641	922.642
W7	-2	1087.167	1087.180
W8	-2	1293.722	1293.749
W9	-2	1445.744	1445.790
W10	-3	1059.842	1059.806
W11	-3	1156.191	1156.169
W12	-3	1260.543	1260.555
W13	-4	1027.418	1027.463
W14	-4	1105.683	1105.677
W15	-4	1183.947	1183.921
a2-A	-1	426.080	426.096
a3-A	-1	739.137	739.131
a4-G	-1	1052.195	1052.213
a5-A	-1	1381.247	1381.230
a6-C	-2	846.648	846.658
a7-C	-2	991.171	991.168
a9-X	-2	1287.717	1287.744
a10-G	-2	1494.272	1494.255
a11-G	-2	1658.798	1658.673
a12-C	-3	1215.213	1215.224
a13-G	-3	1311.562	1311.538

Table S9. Predicted and observed *m/z* for MS/MS fragmentation patterns displayed in Figure S25 of G 16mer in the reaction of HF with AlkB. Predicted CID fragments are shown in Figure S29.

Fragment	**Charge**	**Theoretical *m/z***	**Observed *m/z***
W5	-2	758.115	758.124
W6	-2	922.641	922.671
W8	-2	1251.693	1251.777
W9	-2	1403.716	1403.682
W10	-3	1031.823	1031.694
W11	-3	1128.172	1128.065
W13	-4	1006.404	1006.441
W15	-4	1162.933	1162.906
a2-A	-1	426.080	426.095
a4-G	-1	1052.195	1052.191
a5-A	-1	1381.247	1381.210
a7-C	-2	991.171	991.166
a9-X	-3	858.142	858.118
a11-G	-3	1077.510	1077.551
a12-C	-3	1187.194	1187.252
a13-G	-3	1283.543	1283.532

Table S10. Predicted and observed *m/z* for MS/MS fragmentation patterns displayed in Figure S26 of HO-HF 16mer in the reaction of HF with AlkB. Predicted CID fragments are shown in Figure S29.

Fragment	**Charge**	**Theoretical *m/z***	**Observed *m/z***
W1	-1	306.048	306.041
W2	-1	595.094	595.150
W3	-1	899.139	899.129
W5	-2	758.115	758.105
W6	-2	922.641	922.645
W7	-2	1087.167	1087.146
W8	-3	867.477	867.452
W9	-3	968.825	968.846
W10	-3	1065.174	1065.226
W13	-4	1031.417	1031.465
W14	-4	1109.682	1109.703
a2-A	-1	426.080	426.079
a3-A	-1	739.137	739.120
a4-G	-1	1052.195	1052.189
a5-A	-1	1381.247	1381.172
a6-C	-2	846.648	846.609
a10-G	-3	1001.177	1001.194
a11-G	-3	1110.861	1110.877
a12-C	-3	1220.545	11220.484
a13-G	-3	1316.893	1316.910
a14-T	-4	1069.681	1069.618
a15-C	-4	1145.692	1145.667

Table S11. Predicted and observed *m/z* for MS/MS fragmentation patterns displayed in Figure S27 of m4C 16mer in the reaction of m4C with AlkB. Predicted CID fragments are shown in Figure S29.

Fragment	**Charge**	**Theoretical *m/z***	**Observed *m/z***
W1	-1	306.048	306.047
W3	-1	899.139	899.143
W4	-2	613.592	613.603
W5	-2	758.115	758.119
W6	-2	922.641	922.644
W7	-2	1087.167	1087.183
W9	-2	1390.720	1390.729
W10	-2	1535.243	1535.257
W11	-3	1119.508	1119.482
W12	-3	1223.861	1223.833
W13	-3	1333.545	1333.490
W14	-3	1437.897	1437.903
W15	-4	1156.435	1156.678
a2-A	-1	426.080	426.075
a3-A	-1	739.137	739.143
a4-G	-1	1052.195	1052.187
a5-A	-1	1381.247	1381.259
a6-C	-2	846.648	846.677
a7-C	-2	991.171	991.169
a9-X	-2	1287.717	1287.750
a10-G	-2	1439.248	1439.216
a11-G	-2	1603.774	1603.812
a12-C	-2	1768.300	1768.318
a13-G	-3	1274.879	1274.823
a15-C	-4	1114.182	1114.087

Table S12. Predicted and observed *m/z* for MS/MS fragmentation patterns displayed in Figure S28 of C 16mer in the reaction of m4C with AlkB. Predicted CID fragments are shown in Figure S29.

Fragment	**Charge**	**Theoretical *m/z***	**Observed *m/z***
W1	-1	306.048	306.043
W3	-1	899.139	899.127
W4	-2	613.592	613.597
W5	-2	758.115	758.111
W6	-2	922.641	922.652
W7	-2	1087.167	1087.162
W8	-2	1231.690	1231.629
W9	-2	1383.712	1383.684
W10	-3	1018.488	1018.455
W11	-3	1114.836	1114.847
W12	-3	1219.189	1219.179
W13	-3	1328.873	1328.715
W14	-4	1074.667	1074.614
W15	-4	1152.931	1152.882
a2-A	-1	426.080	426.083
a3-A	-1	739.137	739.124
a4-G	-1	1052.195	1052.185
a5-A	-1	1381.247	1381.255
a6-C	-2	846.648	846.656
a7-C	-2	991.171	991.188
a9-X	-3	858.142	858.126
a10-G	-3	954.490	954.555
a11-G	-3	1064.174	1064.229
a13-G	-3	1270.207	1270.372
a14-T	-3	1379.891	1379.838
a15-C	-4	1110.678	1110.655